Available online at www.sciencedirect.com
ScienceDirect
Computers and Structures 85 (2007) 628–644
Computers & Structures
www.elsevier.com/locate/compstruc

Benchmark problems for incompressible fluid flows with structural interactions

Klaus-Jürgen Bathe [a,*], Gustavo A. Ledezma [b]

[a] Massachusetts Institute of Technology, Cambridge, MA 02139, United States
[b] ADINA R&D, Inc., 71 Elton Avenue, Watertown, MA 02472, United States

Received 15 January 2007; accepted 26 January 2007
Available online 29 March 2007

Abstract

Various methods of analysis for the solution of fluid flows with structural interactions have been proposed in the literature, and new techniques are being developed. In these endeavors, to advance the field, thorough evaluations of the procedures are necessary. To help in establishing such evaluations, we present in this paper the solutions of some benchmark problems. The results can be used to evaluate existing and new formulations of incompressible fluid flows with structural interactions.

Keywords: Incompressible fluid flows; Navier–Stokes equations; Fluid–structure interactions; Benchmark problems; ADINA

1. Introduction

During the last years, significant advances have been made in the development and use of computational methods for fluid flows with structural interactions. These advances pertain to the continuous efforts to reach more effective computational techniques, see for example Refs. [1–17], to include more phenomena [18–21] and to develop and assess analysis methods in very difficult problems to solve [22–46]. As seen, valuable applications of fluid–structure interaction analyses are vast in various industries and scientific endeavors. In particular, the automobile and airplane industries need to pursue such analyses. Also, studies in the biomedical sciences often require the modeling of fluid–structure interaction effects. And surely, as the analyses procedures become more effective and more general, the field of applications will further grow because nature does not distinguish between solids and fluids, and engineers and scientists will need to 'simply simulate nature' as it manifests itself in our various environments.

Since there is a need for effective fluid structure interaction analysis procedures, various approaches have been proposed.

In current simulations, arbitrary Lagrangian–Eulerian (ALE) formulations are now widely used. The ALE continuum mechanics formulation is straight-forward; however, there are a number of important computational issues. For the fluid response, a Lagrangian–Eulerian formulation with moving control volumes is used while for the structural response a pure Lagrangian formulation is employed. These descriptions need be coupled in a consistent and accurate manner for the interface conditions. Of course, the usual difficulties to reach accurate solutions in pure fluid flow analyses and in pure structural analyses are also present in ALE formulations of coupled response. However, a major additional and 'practical' difficulty is that in the ALE formulation to describe the fluid flow, the mesh needs to preserve acceptable element geometries throughout the incremental analysis.

The difficulty to preserve in the ALE formulation acceptable element geometries in the fluid mesh, when the structure undergoes large deformations, has been addressed in various research endeavors, see for example Refs. [47,48] and the references therein. In some

* Corresponding author. Tel.: +1 617 253 6645; fax: +1 617 253 2275.
E-mail address: kjb@mit.edu (K.J. Bathe).

0045-7949/$ - see front matter © 2007 Elsevier Ltd. All rights reserved.
doi:10.1016/j.compstruc.2007.01.025

approaches, the fluid mesh nodal coordinates are updated using the nodal displacements obtained by solving structural equations corresponding to springs or solid elements that connect the fluid nodes. These approaches have significant limitations, similar to the simple use of solving the Laplace equation with appropriate boundary conditions. However, if the approach of solving the Laplace equation is used for lines, surfaces and then volumes, a practical algorithm can be developed [4]. While this approach is quite powerful, the modeling effort needed can be large and there are of course limitations regarding the incremental steps that can be used in an analysis.

Instead of moving the nodal points of the fluid mesh by use of an algorithm, completely new meshes to solve for the

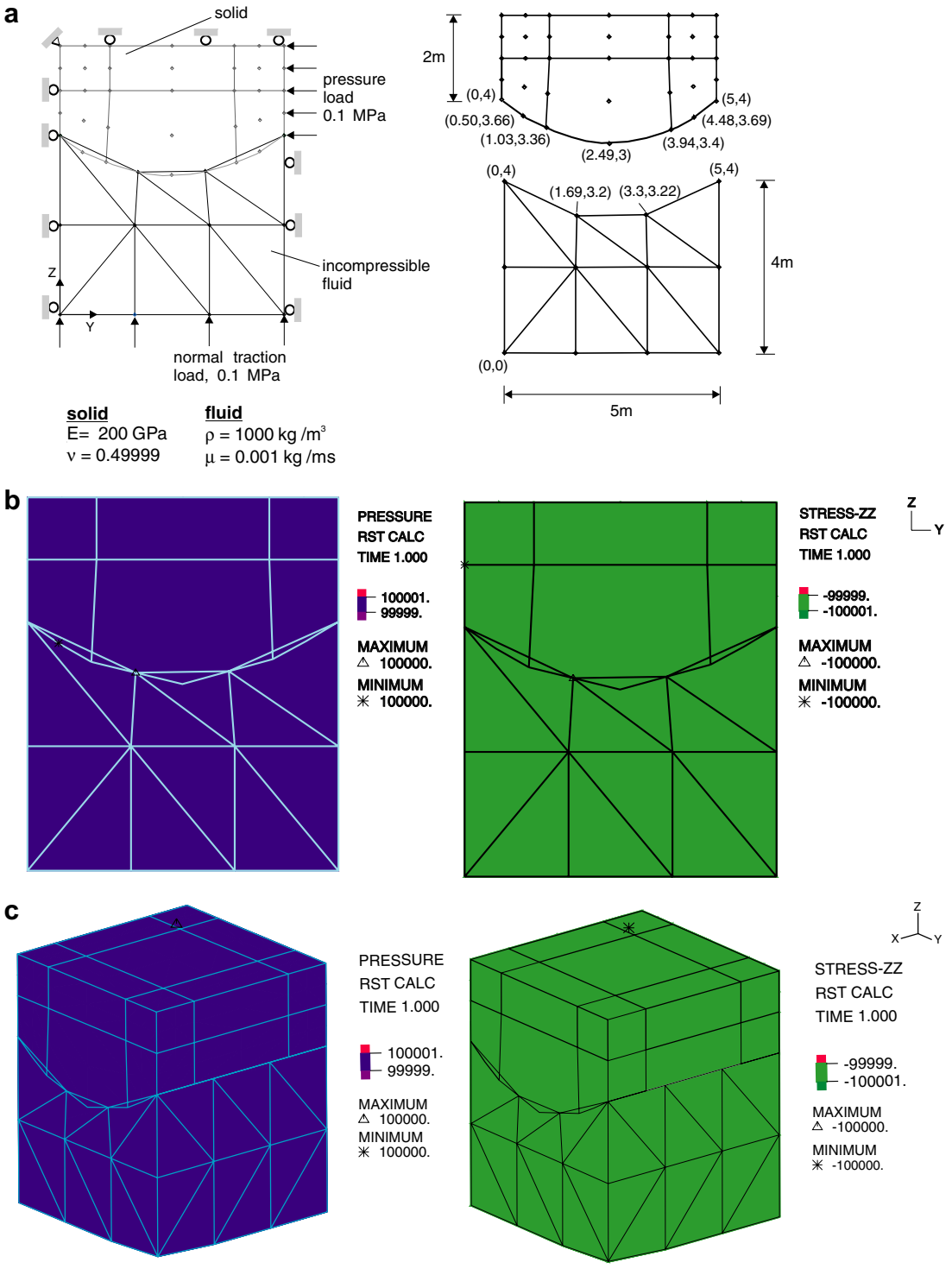

Fig. 1. 2D and 3D FSI patch tests: (a) solid and fluid meshes, and boundary conditions; (b) 2D pressure and stress-zz band plots and (c) 3D pressure and stress-zz band plots.

fluid flow in the incremental analysis may be generated. This approach offers in principle much generality for analysis, but requires efficient and accurate procedures to establish a new mesh for the current fluid domain and the just calculated fluid response. The new fluid mesh needs to be established based on error measures and the fluid response needs to be mapped accurately onto the new mesh. This mapping introduces errors that need to be controlled. The approach is quite attractive for steady-state solutions but in transient analyses the errors introduced by frequent mappings can pollute the response prediction. Therefore this adaptive re-meshing procedure is best used in conjunction with an effective ALE formulation. Then the re-meshing need only be invoked when the other algorithms of the ALE formulation do not succeed in updating the nodal coordinates to obtain an effective fluid mesh.

Since there are these difficulties in reaching effective fluid flow meshes when the fluid flow domains are changing significantly, a number of other formulations have been proposed. The basic idea in 'immersed solid formulations' is to span the complete domain by a (stationary) Eulerian mesh through which the fluid flows and the structure moves, see for example Refs. [14,15] and the references therein. In a simple approach, the structure is simply represented by elastic fibers, or networks of fibers, and forces acting onto the fluid. These solutions can not give an accurate stress response of the structure but only an overall understanding of the fluid flow with the structure embedded in the fluid.

In many FSI analyses we are primarily interested in the structural response, and in particular in the structural stresses that are a result of the fluid interacting with the structure. For such problems, immersed solid formulations are currently developed to represent the actual solid continuum moving through the fluid, see Refs. [14,15,49,50]. A difficulty then encountered is the accurate solution of the trac-

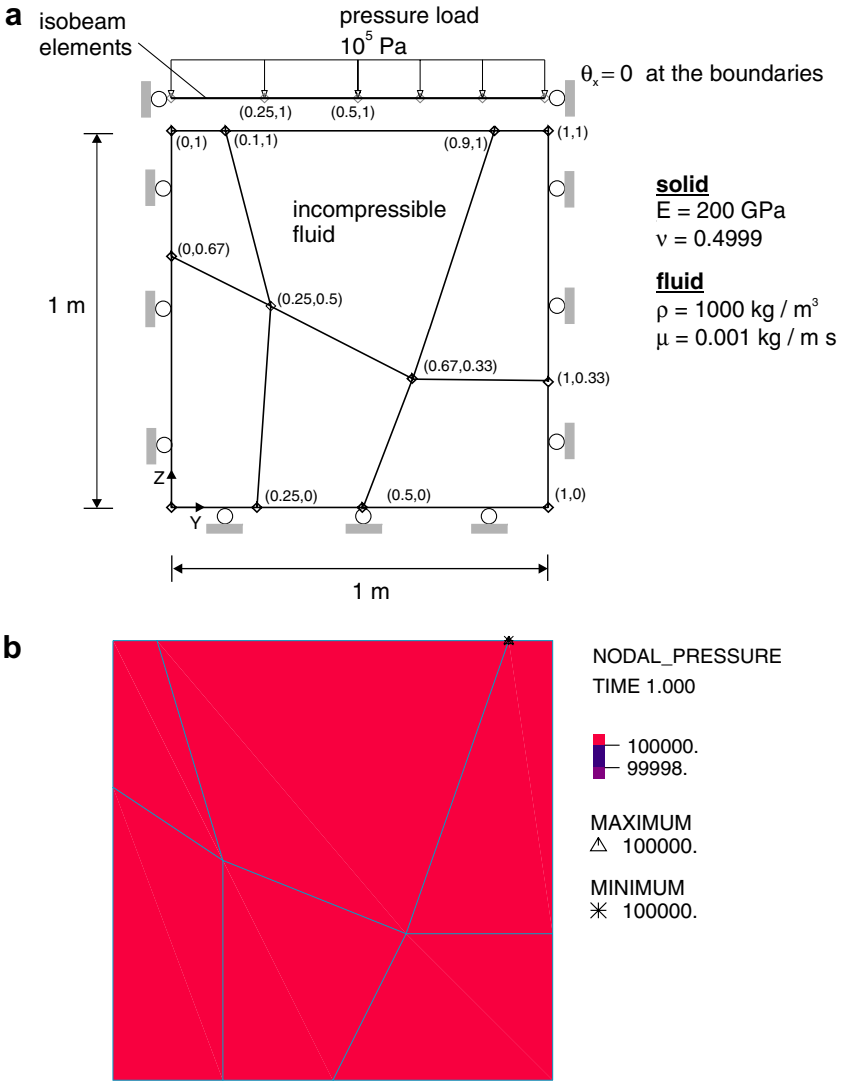

Fig. 2. FSI patch test using two equal-length 3-node and 4-node isoparametric beam elements on the surface of a 2D fluid discretized by quadrilateral elements: (a) solid and fluid meshes, and boundary conditions and (b) pressure band plot in the fluid.

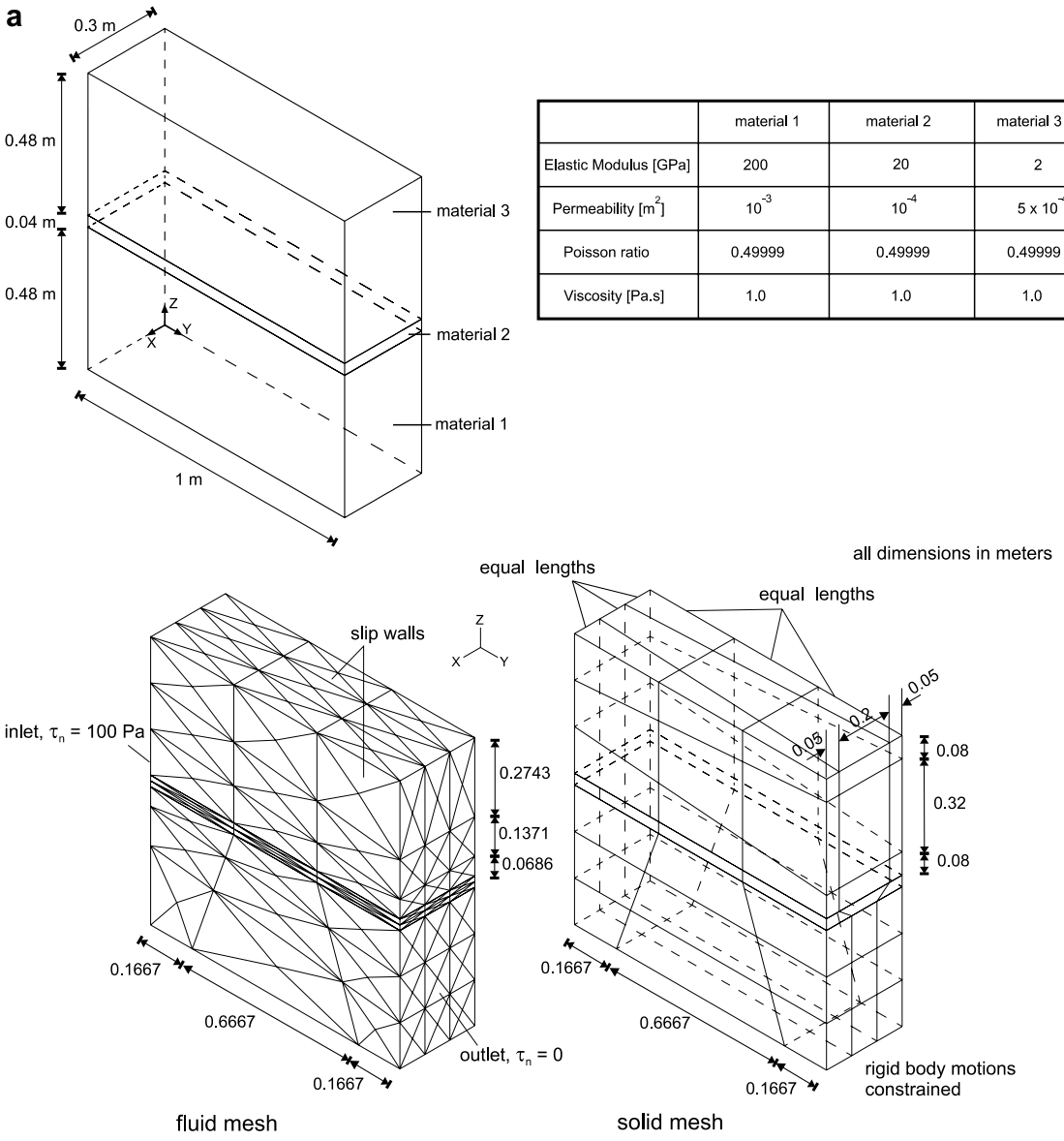

	material 1	material 2	material 3
Elastic Modulus [GPa]	200	20	2
Permeability [m^2]	10^{-3}	10^{-4}	5×10^{-4}
Poisson ratio	0.49999	0.49999	0.49999
Viscosity [Pa.s]	1.0	1.0	1.0

Fig. 3. Porous FSI patch test: (a) model and meshes used and (b) pressure band plot and velocity vectors; *y*-velocity along the *z*-coordinate at the outlet.

tions on the fluid structure boundary and the velocity field near the boundary. Also, fluid flows contained in structural boundaries with large movements can be difficult to solve. Of course, various combinations of ALE formulations and immersed solid formulations can be proposed.

Hence, there are various approaches for fluid structure interaction solutions, which all display some limitations. Since, as mentioned above already, possible applications of fluid structure interaction analyses in various industries and scientific research are wide-spread, and must be expected to increase, significant further advances in the development of fluid structure interaction procedures need be foreseen. These new and possibly improved techniques, however, need to be benchmarked in problem solutions and measured against techniques that are already available.

The main objective in this paper is to present some benchmark solutions that shall help to verify new formulations for fluid structure interaction (FSI) analyses[1] assuming incompressible fluid flow and small or large structural deformations. The benchmark solutions have been obtained using ADINA [3,51,52]. The problems have been selected to not have complex and computationally intensive discretizations but to rather consider 'basic problems' that should be easily solved by an FSI scheme. Since ADINA is widely available, the benchmark solutions can also directly be resolved with the code, if desired, in order to obtain more details regarding the solutions.

In the next sections of the paper we first briefly present the formulations used in ADINA and then we present the various benchmark problems and solutions.

[1] In this paper, we shall use the abbreviation 'FSI' for fluid–structure interactions in which the fluid is governed by the Navier–Stokes equations of isothermal incompressible flows.

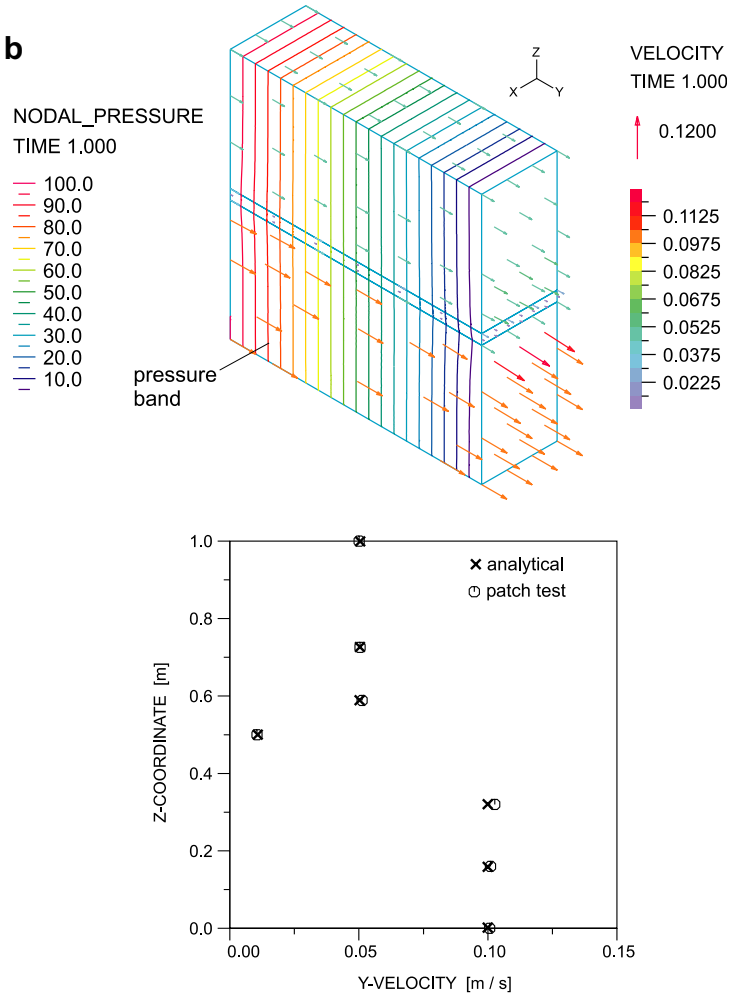

Fig. 3 (*continued*)

We endeavor to present the problems such that the solutions can directly be reproduced using various FSI implementations.

2. Governing equations of fluid flows with structural interactions

In this section, we briefly present the mathematical model of the fluid flow structure interaction problems and the finite element discretizations that we consider.

2.1. Fluid flow equations

We consider an open bounded fluid domain $\Omega \in \mathbb{R}^3$ with boundary $\Gamma = \Gamma_D \cup \Gamma_N \cup \Gamma_i$ where Γ_D and Γ_N are the Dirichlet and Neumann boundaries of the fluid, and Γ_i is the fluid–structure interface boundary. The Navier–Stokes equations of an incompressible, isothermal fluid flow can be written in non-conservative form as

$$\begin{aligned} &\rho\frac{\partial \mathbf{v}}{\partial t} + \rho(\mathbf{v}\cdot\nabla)\mathbf{v} - \nabla\cdot\boldsymbol{\tau} = \mathbf{f}^B \quad \mathbf{x}\in\Omega, \\ &\nabla\cdot\mathbf{v} = 0 \quad \mathbf{x}\in\Omega \end{aligned} \tag{1}$$

subject to the boundary conditions

$$\begin{aligned} &\mathbf{v} = \mathbf{v}_D, \quad \mathbf{x}\in\Gamma_D, \\ &\boldsymbol{\tau}\cdot\mathbf{n} = \mathbf{t}, \quad \mathbf{x}\in\Gamma_N, \\ &\mathbf{v} = \dot{\mathbf{u}}_S^i, \quad \mathbf{x}\in\Gamma_i, \end{aligned} \tag{2}$$

where

$$\boldsymbol{\tau}(\mathbf{v},p) = -p\mathbf{I} + \mu[\nabla\mathbf{v} + (\nabla\mathbf{v})^T] \tag{3}$$

is the stress tensor, μ is the viscosity, $\mathbf{v}$ are the velocities, p is the pressure, $\mathbf{f}^B$ are body forces per unit volume, $\mathbf{v}_D$ are the prescribed velocities on Γ_D, $\dot{\mathbf{u}}_S^i$ are the velocities of the fluid–structure interface Γ_i, $\mathbf{t}$ are the prescribed tractions on Γ_N, $\mathbf{n}$ is the unit outward normal vector to the boundary surface of the fluid, and ρ is the fluid density.

The variational formulation of the Navier–Stokes equations reads [53]

Find $(\mathbf{v},p)\in V\times P$ such that[2]

$$a((\mathbf{v},p),(\mathbf{w},q)) = l(\mathbf{w}) \quad \forall(\mathbf{w},q)\in V_0\times P, \tag{4}$$

[2] We imply throughout the paper to use the appropriate Hilbert spaces or affine manifolds; for details see for example [53,54].

where

$$a((\mathbf{v},p),(\mathbf{w},q)) = \int_\Omega \boldsymbol{\tau}\cdot\nabla\mathbf{w}\,\mathrm{d}\Omega + \int_\Omega q\nabla\cdot\mathbf{v}\,\mathrm{d}\Omega,$$
$$l(\mathbf{w}) = \int_\Omega \mathbf{f}^{\mathrm{B}}\cdot\mathbf{w}\,\mathrm{d}\Omega + \int_{\Gamma_{\mathrm{N}}}\mathbf{t}\cdot\mathbf{w}\,\mathrm{d}\Gamma - \int_\Omega \rho\frac{\partial\mathbf{v}}{\partial t}\cdot\mathbf{w}\,\mathrm{d}\Omega - \int_\Omega \rho(\mathbf{v}\cdot\nabla)\mathbf{v}\cdot\mathbf{w}\,\mathrm{d}\Omega. \quad (5)$$

with $l(\mathbf{w})$ also a function of $\mathbf{v}$.

Of course, the coupling between the fluid and the structure must satisfy the conditions of compatibility and traction equilibrium at the fluid–structure interface. In our solutions, the displacements of the structure are imposed onto the fluid–structure interface of the fluid domain, i.e.,

$$\mathbf{u}(t) = \mathbf{u}_{\mathrm{S}}^{\mathrm{i}}(t), \quad \mathbf{x}\in\Gamma_{\mathrm{i}} \quad (6)$$

and hence the fluid domain is a function of the structural displacements, $\Omega = \Omega(\mathbf{u}_{\mathrm{S}})$.

These are the basic governing equations of the fluid flows we consider, and can be used to derive the equations for related flow conditions, such as flow through porous media and slightly compressible flow.

2.2. Solid equations

We consider an open bounded domain $\Omega_{\mathrm{S}}\in\mathbb{R}^3$ of a solid with boundary $\Gamma_{\mathrm{S}} = \Gamma_{\mathrm{D}}^{\mathrm{S}}\cup\Gamma_{\mathrm{N}}^{\mathrm{S}}\cup\Gamma_{\mathrm{i}}$ where $\Gamma_{\mathrm{D}}^{\mathrm{S}}$ and $\Gamma_{\mathrm{N}}^{\mathrm{S}}$ are the Dirichlet and Neumann boundaries of the solid, and Γ_{i} is the fluid–structure interface boundary. The solid response is described using a Lagrangian formulation where the solid can of course include structural behavior as described by beams, plates, or shells. The solid or structure can be subjected to large deformations and rotations.

Considering a general 3D-nonlinear response, the governing equilibrium equations are

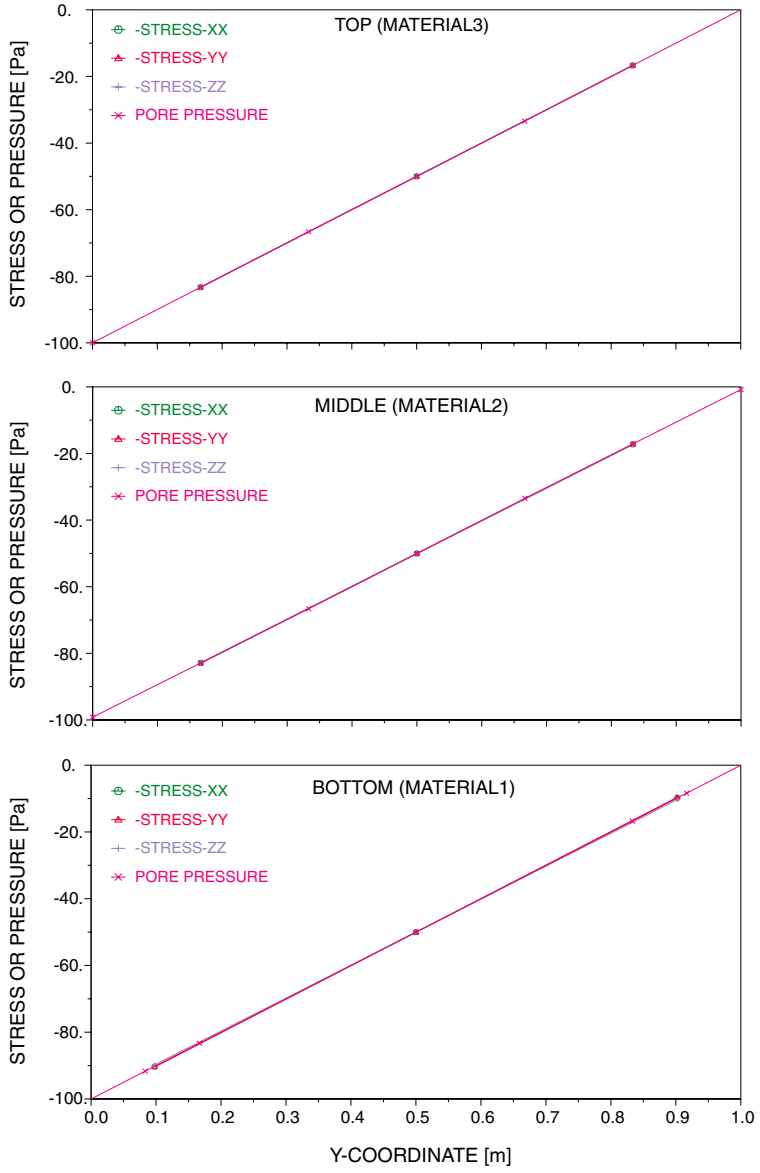

Fig. 4. Porous FSI patch test. Solid model pore pressure and stresses along the y axis. The stresses are plotted at the integration points.

$$\nabla \cdot \boldsymbol{\tau}_S + \mathbf{f}_S^B = \rho_S \frac{\partial^2 \mathbf{u}_S}{\partial t^2}, \quad \mathbf{x} \in \Omega_S, \tag{7}$$

with the boundary conditions

$$\begin{aligned} &\mathbf{u}_S = \mathbf{u}_S^D, \quad \mathbf{x} \in \Gamma_D^S, \\ &\boldsymbol{\tau}_S \cdot \mathbf{n}_S = \mathbf{t}_S, \quad \mathbf{x} \in \Gamma_N^S, \\ &\boldsymbol{\tau}_S \cdot \mathbf{n}_S = -\boldsymbol{\tau} \cdot \mathbf{n} + \mathbf{t}_S^i, \quad \mathbf{x} \in \Gamma_i, \end{aligned} \tag{8}$$

where $\boldsymbol{\tau}_S$ is the Cauchy stress tensor, $\mathbf{f}_S^B$ are body forces per unit volume, $\mathbf{u}_S$ are the unknown displacements, ρ_S is the solid density, $\mathbf{t}_S$ are tractions applied on Γ_N^S, $\mathbf{t}_S^i$ are externally applied tractions to the interface boundary Γ_i, and $\mathbf{n}_S$ is the unit outward normal vector to the boundary surface of the structure. The stresses are of course evaluated using the relevant constitutive relations. We note that in Eq. (8) the traction equilibrium between the fluid and the structure is imposed on Γ_i.

The variational formulation of this problem can be written as [53]

Find $\mathbf{u}_S \in V_S$ such that

$$a_S(\mathbf{u}_S, \mathbf{v}_S) = l_S(\mathbf{v}_S) \quad \forall \mathbf{v}_S \in V_{0,S}, \tag{9}$$

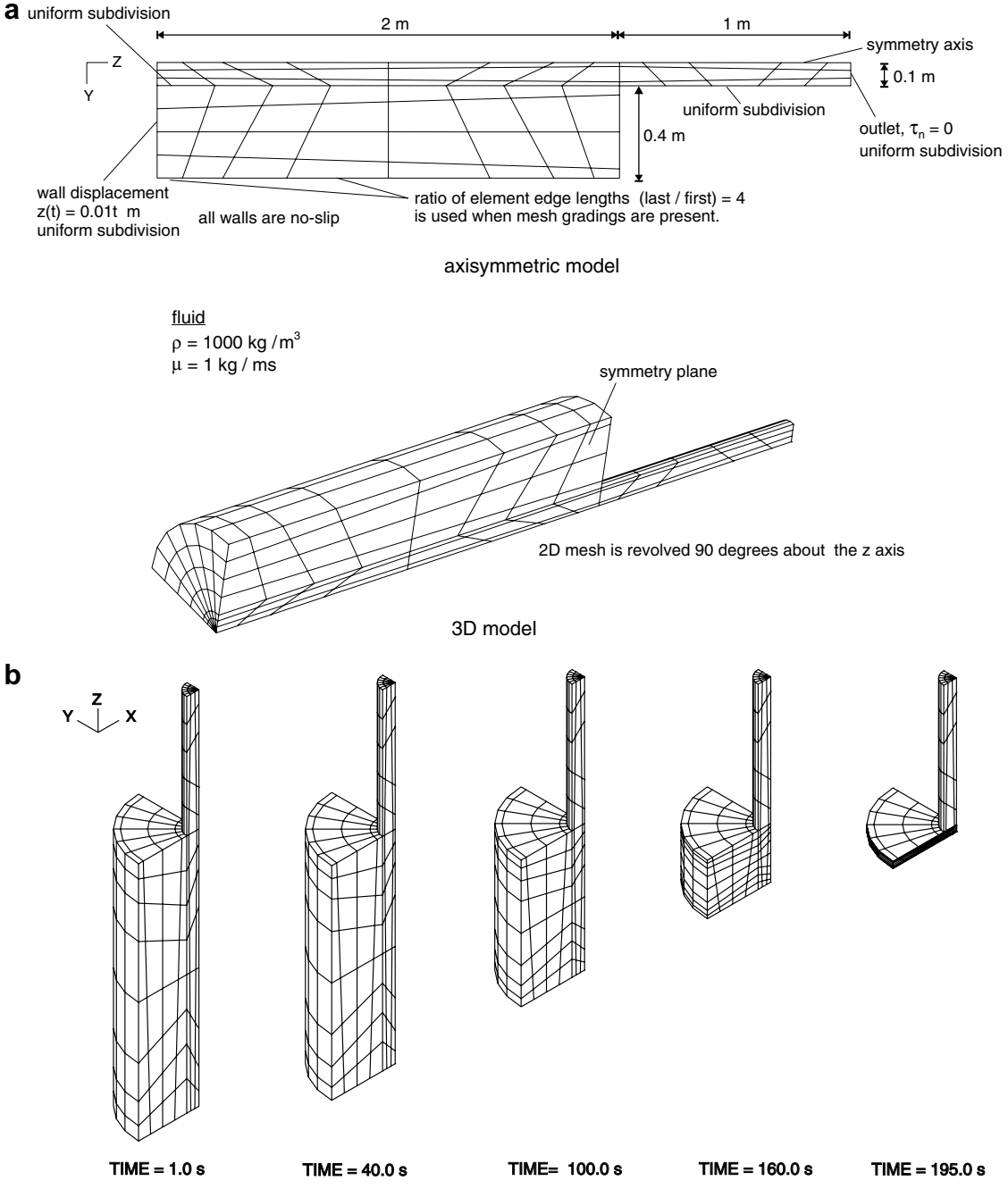

Fig. 5. ALE low *Re* flow test: (a) axisymmetric and 3D model details and (b) time history of the 3D coarse mesh.

where

$$a_S(\mathbf{u}_S, \mathbf{v}_S) = \int_{\Omega_S} \boldsymbol{\tau}_S \cdot \boldsymbol{\varepsilon}_S \, d\Omega_S,$$

$$l_S(\mathbf{v}_S) = \int_{\Omega_S} \mathbf{f}_S^B \cdot \mathbf{v}_S \, d\Omega_S + \int_{\Gamma_N^S} \mathbf{t}_S \cdot \mathbf{v}_S \, d\Gamma + \int_{\Gamma_i} (\mathbf{t}_S^i - \boldsymbol{\tau} \cdot \mathbf{n}) \cdot \mathbf{v}_S \, d\Gamma - \int_{\Omega_S} \rho_S \ddot{\mathbf{u}}_S \cdot \mathbf{v}_S \, d\Omega_S \tag{10}$$

and $\boldsymbol{\varepsilon}_S$ is the strain tensor corresponding to $\mathbf{v}_S$.

The above variational equation directly gives the displacement-based finite element formulations, but for many analyses mixed finite element formulations are more effective. Mixed formulations can be derived by extending the variational formulation in Eq. (9), see for example Refs. [53,54].

2.3. Coupling between fluid flow and solids

The coupling between the fluid and the structure is based on an arbitrary-Lagrangian–Eulerian formulation for the fluid that is coupled to the Lagrangian formulation of the structure [3]. Using the variational formulations for the fluid flow problem and the structural problem, the nonlinear coupled problem can be written in compact form as

Find $\{\mathbf{v}, p, \mathbf{u}_S\} \in \mathscr{V} = V \times P \times V_S$ such that

$$a((\mathbf{v}, p), (\mathbf{w}, q)) + a_S(\mathbf{u}_S, \mathbf{v}_S) = l(\mathbf{w}) + l_S(\mathbf{v}_S) \quad \forall \{\mathbf{w}, q, \mathbf{v}_S\} \in \mathscr{V}_0, \qquad \mathscr{V}_0 = V_0 \times P \times V_{0,S} \tag{11}$$

This nonlinear variational problem describes a fully coupled fluid flow structure interaction problem. The fluid domain, on which $a((\cdot,\cdot),(\cdot,\cdot))$ is defined, depends on the structural displacements $\mathbf{u}_S$.

2.4. Solution of governing FSI continuum equations

The governing equations of the FSI response, given in Eq. (11), are discretized and solved in ADINA using for solids and structures the element formulations published in Ref. [53] and for the fluid flow the element formulations

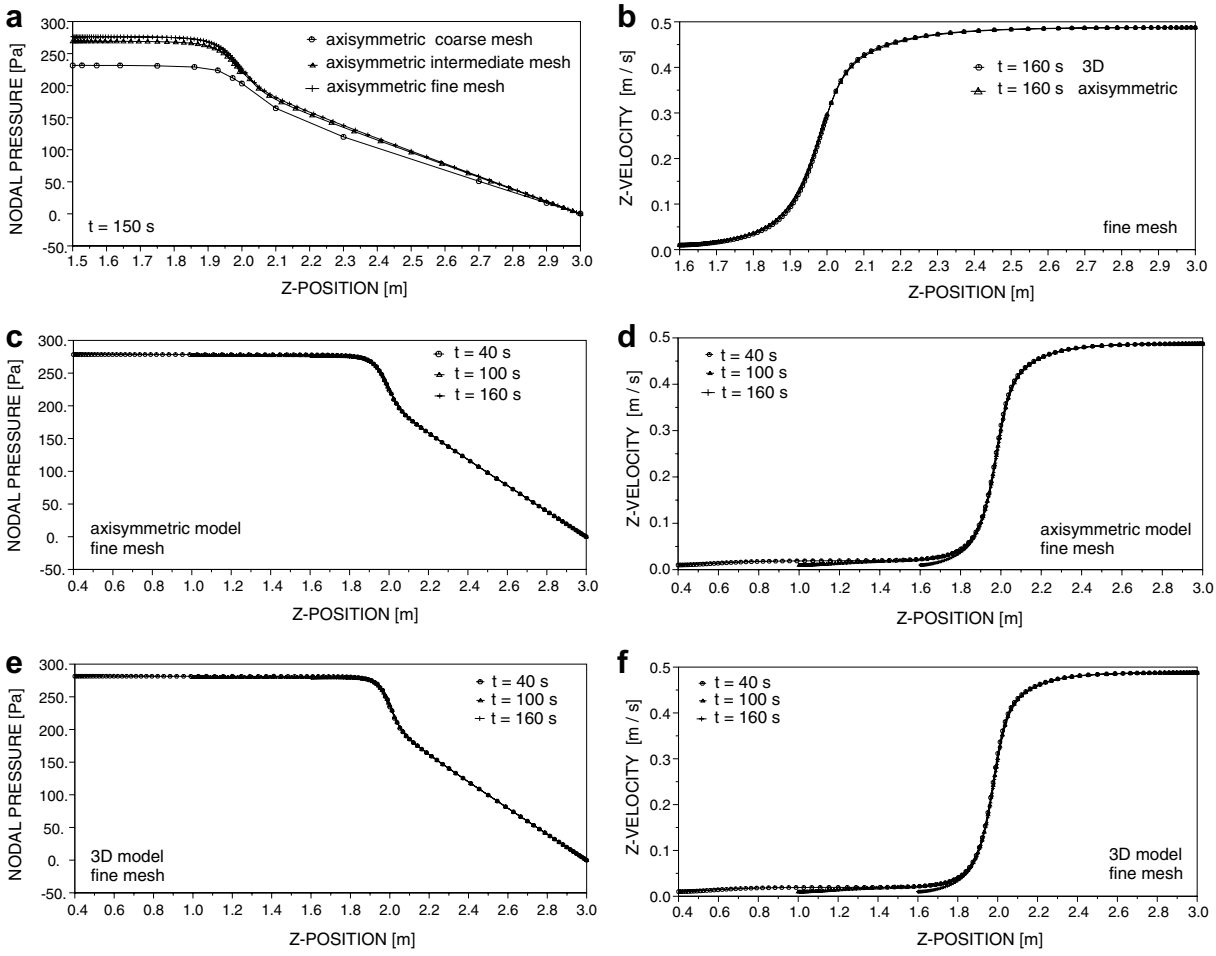

Fig. 6. ALE low *Re* flow test. Axisymmetric and 3D model pressure and z-velocity results along the axis: (a) axisymmetric model mesh refinement; (b) direct comparison of the z-velocity for the axisymmetric and 3D models; (c) nodal pressure in the axisymmetric model; (d) z-velocity in the axisymmetric model; (e) nodal pressure in the 3D model; and (f) z-velocity in the 3D model.

presented in Refs. [3,55]. The flow-condition-based interpolation (FCBI) approach used for solution of incompressible flows has also been studied further in Refs. [56–58]. As discussed in Refs. [55–58], the objective in the FCBI formulations is to have good stability and sufficient accuracy for FSI solutions.

As mentioned already above, specific attention needs to be given to the coupling between the solid and structural domains and the fluid domains. With the method used in ADINA arbitrary meshes can be employed for the different regions, which is important in engineering practice. Namely, the solution of the fluid response may require certain mesh densities that in general must be quite different from the mesh densities used to solve for the structural response. The specific coupling employed is described in Ref. [3].

For the purpose of presenting benchmark solutions, the specific iterative scheme used to solve the finite element equations is of course not of importance. However, we should mention that whichever fully coupled solution scheme is used in ADINA, the full coupling is considered by solving the fully coupled algebraic equations obtained from Eq. (11). Since these equations are highly nonlinear, in general, a Newton–Raphson 'outer iteration' is employed. The matrix equations established in each Newton–Raphson step are then solved either directly by a sparse solver (for small systems of equations) or by an 'inner iteration' using a multi-grid solver (for larger systems of equations). At convergence of the Newton–Raphson iterations, the finite element equations established from Eq. (11) have been solved to the accuracy specified by the convergence tolerances used, and only the efficiency

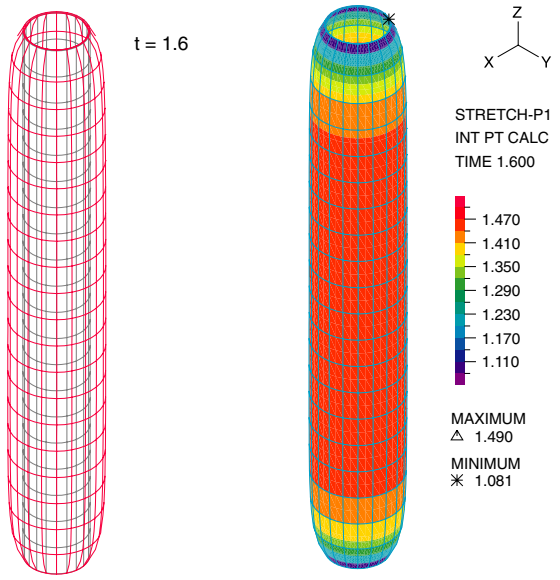

Fig. 8. Mass conservation test. Mesh deformation and maximum principal stretch.

Table 1
Mass conservation test

t	Re	Flow rate [kg/s]		
		$z = 0$ m	$z = 0.5$ m	$z = 1$ m
0.4	31.2	2.45199	2.45198	2.45198
1.0	121.1	9.51151	9.51151	9.51151
1.6	361.7	28.4088	28.4088	28.4088

Flow rates at three different sections along the axis.
The Reynolds number is based on the average velocity at the inlet, $z = 0$ m and the channel inner diameter, $D = 0.1$ m.

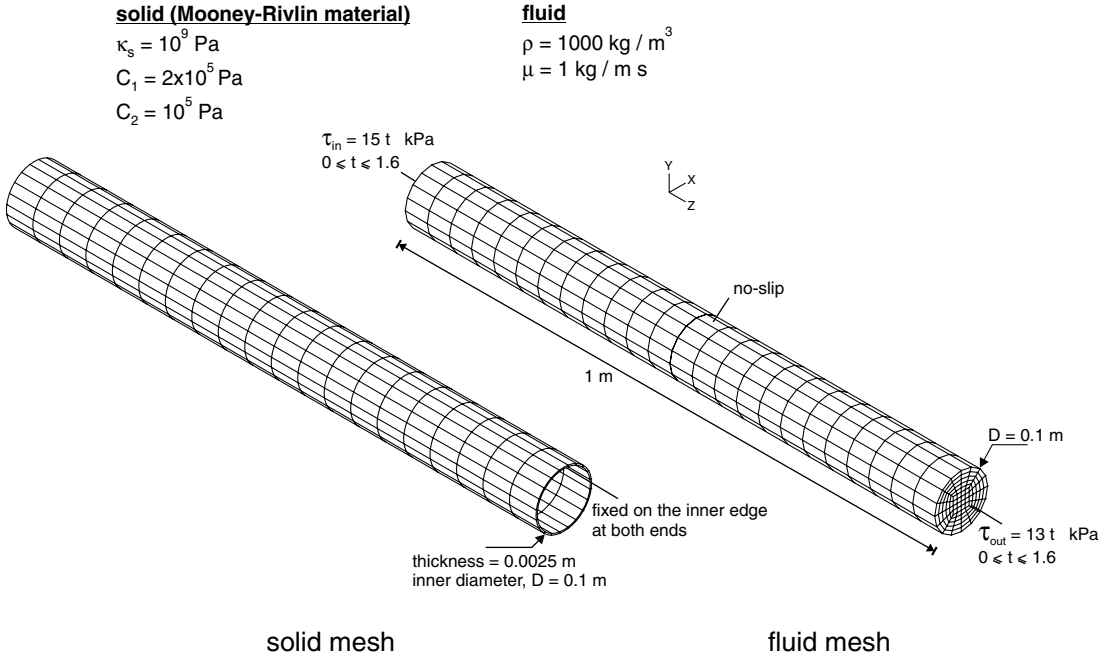

Fig. 7. Mass conservation test. Dimensions, properties and boundary conditions; meshes used.

is affected by the choice of the solution scheme. In the benchmark solutions given below, all convergence tolerances have been set to be tight, so that any error in solving the finite element equations is negligible.

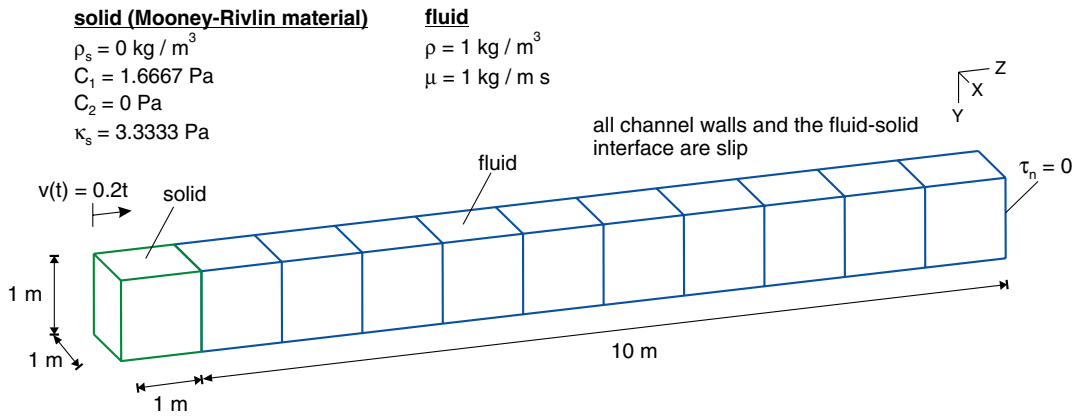

Fig. 9. Strong coupling test. Solid mesh and fluid mesh with 1 and 10 elements respectively. The solid material is confined to stay in the channel.

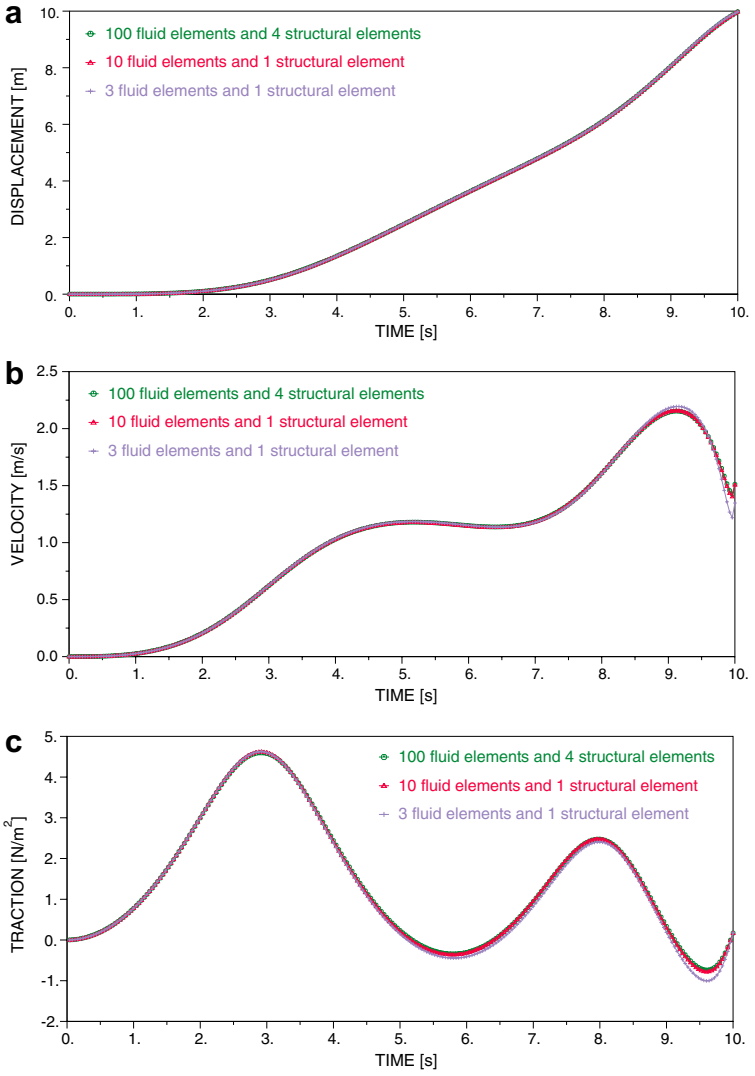

Fig. 10. Strong coupling test results at the fluid–solid interface using three different meshes: (a) displacement in the z-direction; (b) velocity; and (c) traction.

3. Benchmark solutions

In this section we present some benchmark solutions that should be valuable in the evaluations of procedures for FSI analyses. In all transient solutions we use the time integration scheme of Ref. [59].

3.1. FSI patch tests

The patch test is an important means to assess whether an incompatible mesh of elements can represent constant stress conditions [53]. We use the test in FSI analysis schemes to see whether fluid and solid/structural domains, meshed independently and using incompatible meshes, will transmit constant stress conditions.

Fig. 1 shows the 2D patch test and the solution results. Fig. 1 also shows the same patch test but performed in 3D. We should note the curved boundary between the fluid and the solid. The fluid geometrically linear elements overlap the solid geometrically quadratic elements, and of course, the two meshes are totally incompatible at the fluid–solid interface. The patch test is passed in both cases.

Fig. 2 shows another patch test using 4-node and 3-node isoparametric beam elements on the surface of a 2D fluid, discretized by quadrilateral elements. The pressure applied to the beam elements must be exactly transmitted to the fluid, as seen in this test. The same test should of course also be passed in 3D, that is, when shell elements subjected to pressure are resting on the surface of a 3D fluid domain.

Of course, additional patch tests, e.g. using 2-node beam elements, for a numerical assessment can be designed, but the theory underlying the FSI formulation will already tell whether any (relevant) patch test is passed.

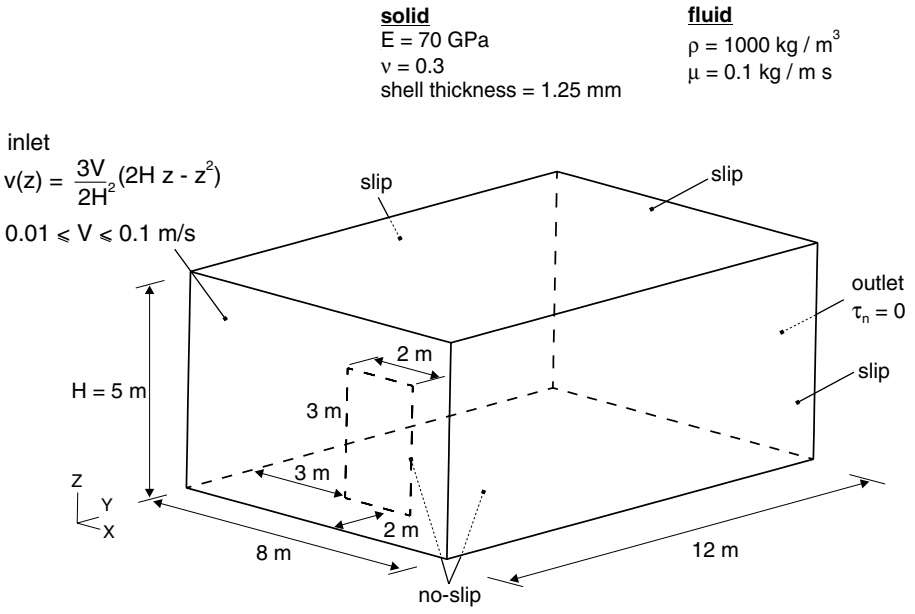

Fig. 11. Shell in steady-state cross flow test. Dimensions and boundary conditions. The shell is fixed at the bottom.

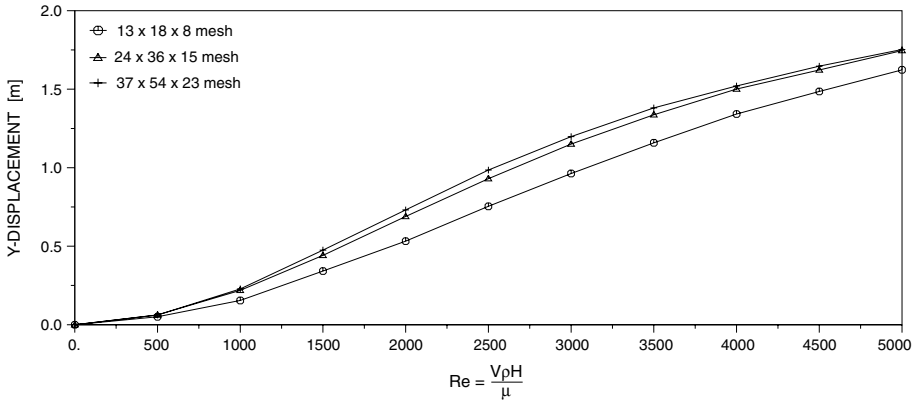

Fig. 12. Tip displacement of the shell as a function of the flow Reynolds number; the number of elements given for each fluid mesh correspond to the *X*, *Y* and *Z*-directions (see Fig. 11).

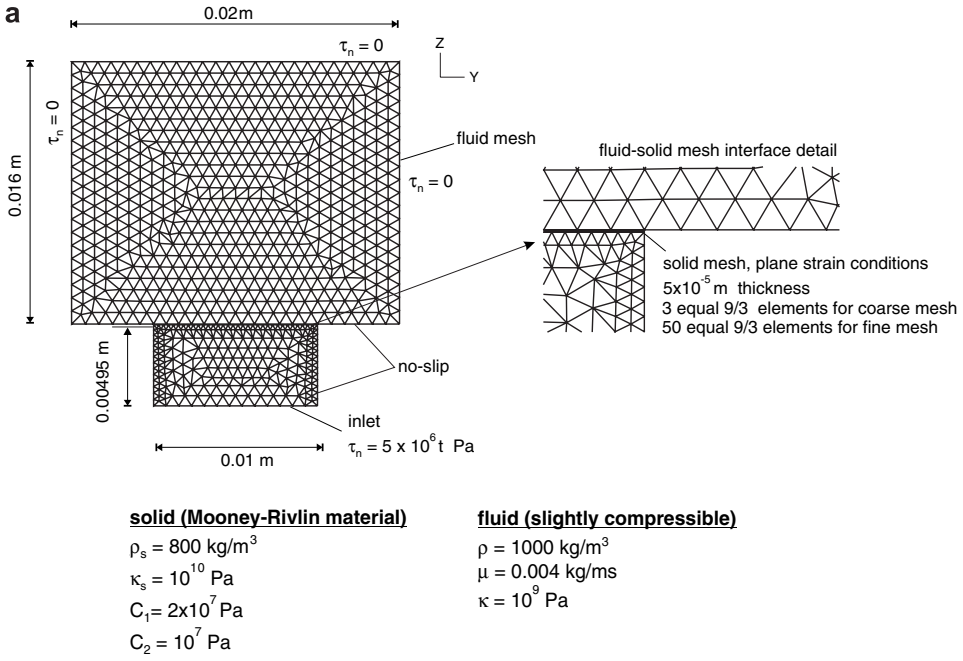

Fig. 13. Large deformation membrane on fluid test: (a) model dimensions and boundary conditions (fine mesh is shown) and (b) time histories of the coarse and fine meshes.

3.2. Porous FSI patch test

Fig. 3 shows the problem solved. Three different stacked porous media are subjected to the same pressure gradient. Hence, with the different permeabilities, the flow velocities in the media need be different. The test is passed if the flow velocities and pressure variations are the analytical values even though distorted elements are used in the meshes. Since velocity discontinuities at the media interfaces are not modeled, small errors in the calculated velocities are acceptable.[3]

Fig. 3 shows the pressure band plot and velocity vectors in the fluid domain, and the *y*-velocity along a vertical line at the outlet. As expected, the velocity varies from one material to the other according to Darcy's law.

Another purpose of this test is to check the accurate transfer of the fluid pressure to the structural model. The stresses in the solid and the pore pressure (given as a negative quantity) are plotted in Fig. 4. These results show that the patch test is passed.

3.3. ALE low *Re* flow test

In low *Re* flows, a discretization should represent the incompressible conditions accurately and hence solve accurately for the pressure and flow velocities. This observation is applicable to the 'element *Re* numbers' and although, overall, a high *Re* flow may be solved, in certain regions (in flow stagnations) the element *Re* numbers may be small. The difficulty of solving for the pressure and velocities accurately in finite difference and finite volume methods was recognized long time ago and staggered mesh points for pressure and velocity assumptions were introduced [60].

The mathematical condition for optimal solutions is that the discretization used must satisfy the inf–sup condition (or the problem must be reformulated to by-pass this condition). The condition is satisfied by the continuum problem in Eq. (11), but is only satisfied by a discretization provided appropriate velocity and pressure interpolations are used [53,61,62]. Analytical investigations have identified elements that satisfy the inf–sup condition, assuming largely uniform meshes; and a numerical inf–sup test has been proposed for discretization schemes not amenable to analytical proofs, considering for example new elements and distorted element meshes [53,63,64].

We present here a problem solution with a moving mesh to test the accuracy in the prediction of pressure and flow velocities as the element size is decreasing.

Fig. 5 shows the problem we consider: a moving wall pushes fluid into a channel with a sudden contraction. The initially distorted element meshes in the axisymmetric and 3D solutions are rather coarse. The finer meshes of distorted elements in the analyses are obtained by simply increasing the number of elements in the axial and radial directions first by a factor of 4 and then by an additional factor of 2. The third mesh is therefore very fine. In each case, specifically, the pressure predictions are of interest,

[3] Of course, velocity discontinuities could be introduced by simply assigning at the interfaces two nodes where now one node is used and then allowing independent tangential 'slip' velocities (but constraining the normal velocities to be continuous). This approach requires in practice more modeling effort.

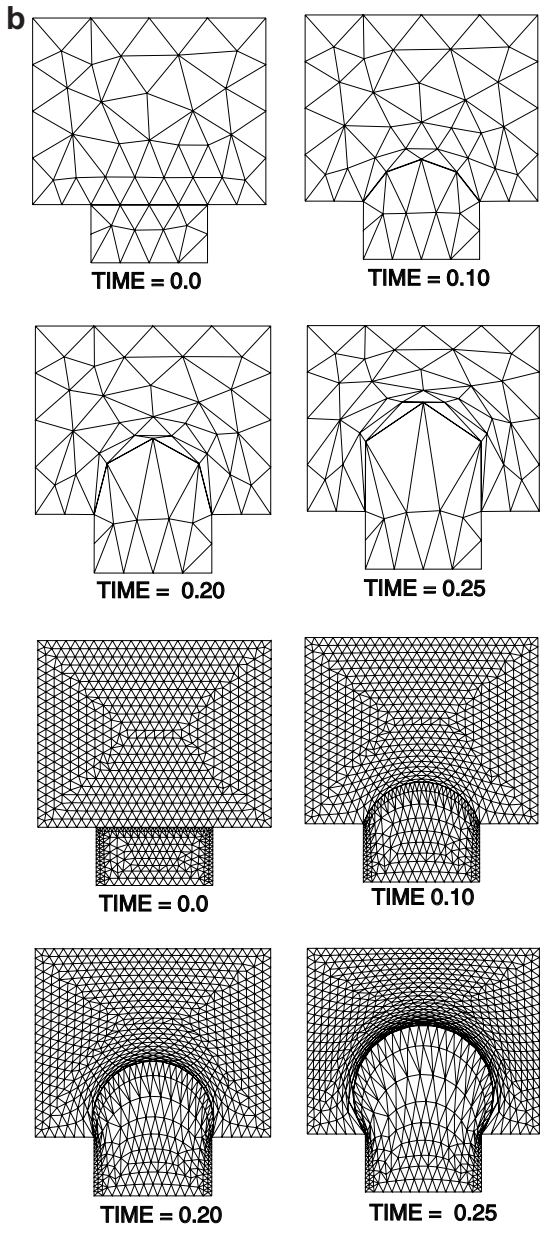

Fig. 13 (*continued*)

that is, whether any oscillations occur. Fig. 5 shows how the 3D coarse mesh is compressed in the analysis. Fig. 6 shows the smooth pressure predictions along the z-axis calculated in this test. The effect of refining the mesh and comparisons between the axisymmetric and 3D test results are also given. The maximum Reynolds number based on the contracted channel diameter is 50.

3.4. Mass conservation test

In CFD solutions, it is of particular importance to satisfy the conservation of mass and momentum conditions 'locally', that is, for local patches of elements, and hence for any section through the flow field. In FSI solutions, this conservation property should also hold for the flow when the boundaries of the fluid mesh move.

Fig. 7 shows the problem we use to test the mass conservation property. The flexible cylindrical channel wall is represented using one layer of 3D 27-node solid elements and the fluid is represented by 3D 8-node elements. Fig. 8 shows the deformation of the channel wall at $t = 1.6$ (see Fig. 7) and also the principal stretch. The mass flow rates calculated at three sections of the channel are listed in Table 1. It is seen that mass conservation is satisfied and hence the test is passed.

3.5. Strong coupling test

The problem considered here is taken from Ref. [65] and is described in Fig. 9. In this transient FSI problem, the coupling between the fluid and the structure is strong, which makes the solution a valuable test. While in Ref. [65] linear conditions are assumed for the solid, we use here for the solid a compressible Mooney–Rivlin material model and assume large deformations [53,66]. However, the problem is still "rather constructed" with the data given.

We present our results using three different meshes: a coarse mesh with three equal 8-node fluid elements and one 8-node 3D solid element; an intermediate mesh, shown in Fig. 9, with 10 equal 8-node fluid elements and one 8-node 3D solid element; and a fine mesh with one hundred equal 8-node fluid elements and four equal 8-node solid elements.

Fig. 10 shows the calculated solutions for all meshes, using $\Delta t = 0.02$ s. Good convergence of the solutions is seen.

3.6. Shell in steady-state cross-flow test

The problem considered here is described in Fig. 11. Similar problems were solved already in Refs. [3,67]. The purpose of this problem solution is to verify the FSI capability when a shell structure undergoes large deformations.

A flexible, initially vertical plate is subjected to flow and undergoes large deformations, which makes the plate structure act like a shell. The shell is always discretized using a mesh of 6×12 equal MITC4 shell elements, while 8-node 3D FCBI elements are used to discretize the fluid domain. Fig. 12 gives the tip displacement of the shell (at the midpoint of the free edge) as a function of the flow Reynolds number when increasingly finer meshes are used. Good convergence of the predicted response is seen.

3.7. Large deformation membrane on fluid test

Fig. 13 shows the problem considered. The purpose of this problem solution is to test the FSI scheme in a large displacement problem when a free-form mesh of triangular elements is used and the mesh nodes are automatically moved.

We solve for the transient response with $\Delta t = 0.001$ s until $t = 0.25$. The membrane undergoes large displacements and large strains. Two meshes, a coarse and a fine

fluid mesh (with also coarse and fine structural meshes) are used. The time evolutions of the nodal positions in the fluid meshes automatically calculated throughout the incremental response are shown in Fig. 13.

The maximum displacement and stretch of the membrane in the incremental solution are shown Fig. 14. It is seen that the coarse mesh solution is quite close to the fine mesh solution.

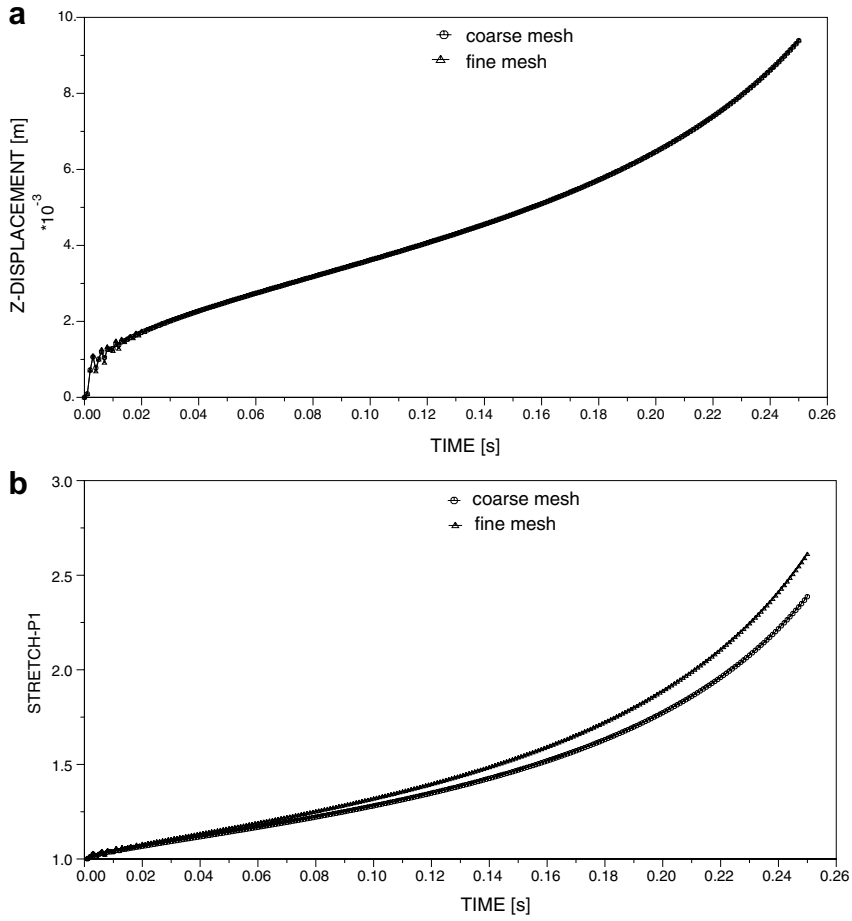

Fig. 14. Large deformation membrane on fluid test: (a) vertical displacement of the membrane center and (b) principal maximum stretch of the element located at the membrane center.

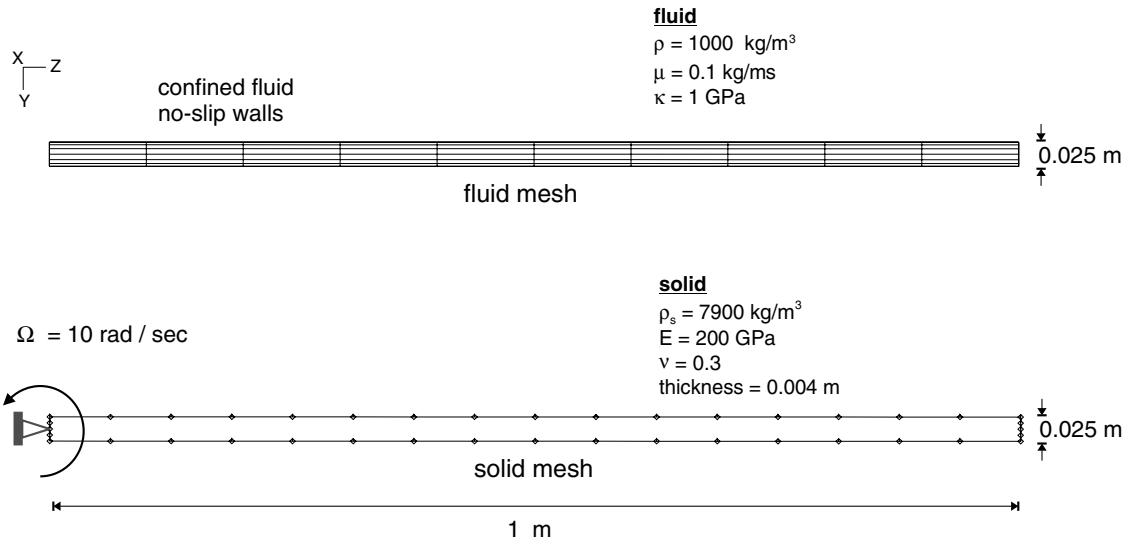

Fig. 15. Transient rotation of channel with fluid flow test. Meshes and boundary conditions.

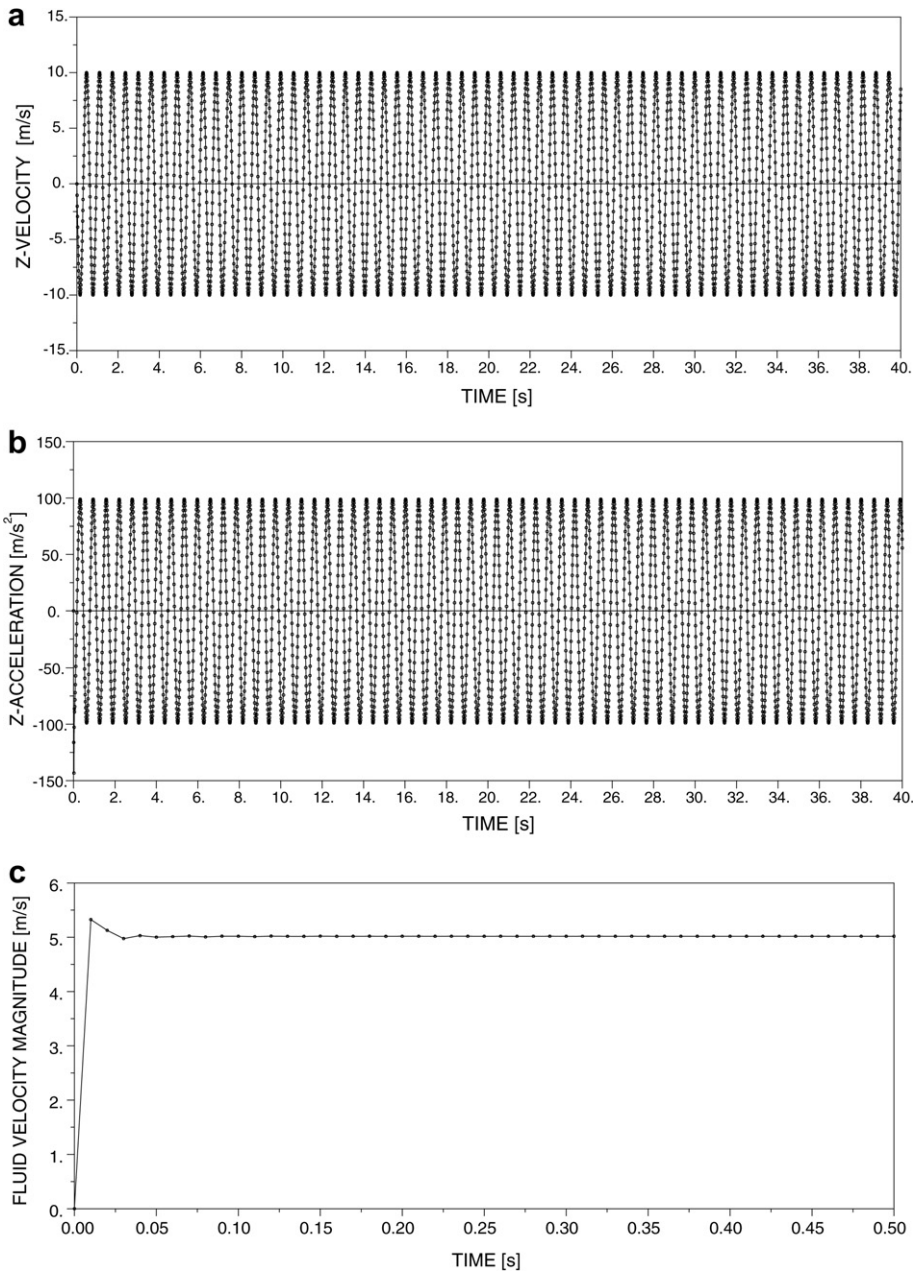

Fig. 16. Transient rotation of channel with fluid flow test: (a) channel tip velocity in the z-direction; (b) channel tip acceleration in the z-direction and (c) fluid velocity magnitude at the center of the channel.

3.8. Transient rotation of channel with fluid flow test

The large deformation FSI problem we consider is shown in Fig. 15. A water-filled steel channel rotates through the full 360°. For the complete time span, a rotation of 10 rad/s is prescribed at the left end. The objective in this problem solution is to test the FSI scheme for large rotations of the fluid mesh.

The fluid mesh consists of 4-node elements and the structure is represented by 3-node isoparametric beam elements.

Fig. 16 shows the calculated tip velocity and acceleration of the channel using $\Delta t = 0.01$ s. The figure also shows the magnitude of the fluid velocity at the center of the channel.

It may be noted that this problem is an extension of the pendulum problem considered in Ref. [59], but since the rotation is prescribed, various time integration schemes can be used for solution. We use the problem here to *only* test whether the rotation of the fluid mesh is achieved correctly.

4. Concluding remarks

The objective in this paper was to present some benchmark problems and their solutions for fluid flow structure interaction analyses. We endeavored to present the problems and the solutions in such a way that they can be directly used for basic testing of FSI solution schemes.

The problems considered are 'basic' problems and do not involve large finite element models. We gave emphasis to those features of FSI solution schemes that couple structural finite element models and fluid flow models. Some of the problems are quite rich in response (in particular, when changed in certain respects) and could benefit from further studies.

We considered in this paper only isothermal incompressible fluid flows, but of course benchmark problems and their solutions will also be valuable for FSI involving significant thermal effects and for compressible flows with structural interactions. These are topics for further valuable publications.

Acknowledgement

The authors thank Dr. N. Elabbasi of ADINA R&D for valuable comments on this paper.

References

[1] Bathe KJ, editor. Computational Fluid and Solid Mechanics 2003. Elsevier; 2003.
[2] Bathe KJ, editor. Computational Fluid and Solid Mechanics 2005. Elsevier; 2005.
[3] Bathe KJ, Zhang H. Finite element developments for general fluid flows with structural interactions. Int J Numer Methods Eng 2004;60:213–32.
[4] Bathe KJ, Zhang H, Ji S. Finite element analysis of fluid flows fully coupled with structural interactions. Comput Struct 1999;72:1–16.
[5] Unger R, Haupt MC, Horst P. Application of Lagrange multipliers for coupled problems in fluid and structural interactions. Comput Struct 2007;85(11–14):796–809.
[6] Tang L, Païdoussis M. A fluid elastic model for the dynamics of cantilevered plates with an additional spring support in axial flow. Comput Struct 2007;85(11–14):1089–96.
[7] Birk C, Ruge P. Representation of radiation damping in a dam-reservoir interaction analysis based on a rational stiffness approximation. Comput Struct 2007;85(11–14):1152–63.
[8] Chattot J-J. Helicoidal vortex model for wind turbine aeroelastic simulation. Comput Struct 2007;85(11–14):1072–9.
[9] Antoci C, Gallati M, Sibilla S. Numerical simulation of fluid–structure interaction by SPH. Comput Struct 2007;85(11–14):879–90.
[10] Vierendeels J, Lanoye L, Degroote J, Verdonck P. Implicit coupling of partitioned fluid–structure interaction problems with reduced order models. Comput Struct 2007;85(11–14):970–6.
[11] Parrinello F, Borino G. Lagrangian finite element modeling of dam–fluid interaction: accurate absorbing boundary conditions. Comput Struct 2007;85(11–14):932–43.
[12] Kayser-Herold O, Matthies HG. A unified least-squares formulation for fluid–structure interaction problems. Comput Struct 2007; 85(11–14):998–1011.
[13] Guilkey JE, Harman TB, Banerjee B. An Eulerian–Lagrangian approach for simulating explosions of energetic devices. Comput Struct 2007;85(11–14):660–74.
[14] Wang XS. An iterative matrix-free method in implicit immersed boundary/continuum methods. Comput Struct 2007;85(11–14): 739–48.
[15] Tai CH, Liew KM, Zhao Y. Numerical simulation of 3D fluid–structure interaction flow using an immersed object method with overlapping grids. Comput Struct 2007;85(11–14):749–62.
[16] Morgenthal G, Walther JH. An immersed interface method for the vortex-in-cell algorithm. Comput Struct 2007;85(11–14):712–26.
[17] Lee K, Noguchi H, Koshizuka S. Fluid–shell structure interaction analysis by coupled particle and finite element method. Comput Struct 2007;85(11–14):688–97.
[18] Frangi A, Frezzotti A, Lorenzani S. On the application of the BGK kinetic model to the analysis of gas–structure interactions in MEMS. Comput Struct 2007;85(11–14):810–7.
[19] Pan TW, Glowinski R, Hou S. Direct numerical simulation of pattern formation in a rotating suspension of non-Brownian settling particles in a fully filled cylinder. Comput Struct 2007;85(11–14):955–69.
[20] Melnik R, Mahapatra R. Coupled effects in quantum dot nanostructures with nonlinear strain and bridging modelling scales. Comput Struct 2007;85(11–14):698–711.
[21] Han K, Feng YT, Owen DRJ. Coupled Lattice Boltzmann and discrete element modelling of fluid–particle interaction problems. Comput Struct 2007;85(11–14):1080–8.
[22] Kaazempur-Mofrad MR, Bathe M, Karcher H, Younis HF, Seong HC, Shim EB, et al. Role of simulation in understanding biological systems. Comput Struct 2003;81:715–26.
[23] Shangguan WB, Lu ZH. Experimental study and simulation of a hydraulic engine mount with fully coupled fluid structure interaction finite element analysis model. Comput Struct 2004;82:1751–71.
[24] Moghani T, Butler JP, Lin JL, Loring SH. Finite element simulation of elasto-hydrodynamic lubrication of soft biological tissues. Comput Struct 2007;85(11–14):1114–20.
[25] Scotti CM, Finol EA. Compliant biomechanics of abdominal aortic aneurysms: a fluid–structure interaction study. Comput Struct 2007; 85(11–14):1097–113.
[26] Cavagna L, Quaranta G, Mantegazza P. Application of Navier–Stokes simulations for aeroelastic stability assessment in transonic regime. Comput Struct 2007;85(11–14):818–32.
[27] Kambouchev N, Noels L, Radovitzky R. Numerical simulation of the fluid–structure interaction between air blast waves and free-standing plates. Comput Struct 2007;85(11–14):923–31.
[28] Cirak F, Deiterding R, Mauch SP. Large-scale fluid–structure interaction simulation of viscoplastic and fracturing thin shells subjected to shocks and detonations. Comput Struct 2007; 85(11–14):1049–65.
[29] Liu A, Rugonyi S, Pentecost JO, Thornburg KL. Finite element modeling of blood flow-induced mechanical forces in the outflow tract of chick embryonic hearts. Comput Struct 2007;85(11–14): 727–38.
[30] Thomson SL, Mongeau L, Frankel SH. Flow over a membrane-covered, fluid-filled cavity. Comput Struct 2007;85(11–14):1012–9.
[31] Karagiozis KN, Païdoussis MP, Amabili M. Effect of geometry on the stability of cylindrical clamped shells subjected to internal fluid flow. Comput Struct 2007;85(11–14):645–59.
[32] Yang C, Tang D, Haber I, Geva T, del Nido PJ. In vivo MRI-based 3D FSI RV/LV models for human right ventricle and patch design for potential computer-aided surgery optimization. Comput Struct 2007;85(11–14):988–97.
[33] Lim K-M, Li H. A coupled boundary element/finite difference method for fluid–structure interaction with application to dynamic analysis of outer hair cells. Comput Struct 2007;85(11–14):911–22.
[34] Violette R, de Langre E, Szydlowski J. Computation of vortex-induced vibrations of long structures using a wake oscillator model: comparison with DNS and experiments. Comput Struct 2007;85(11–14):1134–41.
[35] Modarres-Sadeghi Y, Païdoussis M, Semler C. The nonlinear behaviour of a slender flexible cylinder pinned or clamped at both ends and subjected to axial flow. Comput Struct 2007;85(11–14): 1121–33.
[36] Natarajan RN, Williams JR, Lavender SA, Andersson GBJ. Poro-elastic finite element model to predict the failure progression in a lumbar disc due to cyclic loading. Comput Struct 2007;85(11–14): 1142–51.
[37] Luo X, Calderhead B, Liu H, Li W. On the initial configurations of collapsible channel flow. Comput Struct 2007;85(11–14):977–87.

[38] Tijsseling AS. Water hammer with fluid–structure interaction in thick-walled pipes. Comput Struct 2007;85(11–14):844–51.
[39] Mitran SM. Metachronal wave formation in a model of pulmonary cilia. Comput Struct 2007;85(11–14):763–74.
[40] Baylot JT, Bevins TL. Effect of responding and failing structural components on the airblast pressures and loads on and inside of the structure. Comput Struct 2007;85(11–14):891–910.
[41] Witteveen JAS, Sarkar S, Bijl H. Modeling physical uncertainties in dynamic stall induced fluid–structure interaction of turbine blades using arbitrary polynomial chaos. Comput Struct 2007;85(11–14): 866–78.
[42] Dailey HL, Yalcin HC, Ghadiali SN. Fluid–structure modeling of flow-induced alveolar epithelial cell deformation. Comput Struct 2007;85(11–14):1066–71.
[43] He Z, Epureanu BI, Pierre C. Parametric study of the aeroelastic response of mistuned bladed disks. Comput Struct 2007;85(11–14): 852–65.
[44] Petrini F, Giuliano F, Bontempi F. Comparison of time domain techniques for the evaluation of the response and the stability in long span suspension bridges. Comput Struct 2007;85(11–14): 1032–48.
[45] Wang X, Wang LB. Dynamic analysis of a water-soil-pore water coupling system. Comput Struct 2007;85(11–14):1020–31.
[46] Salvatori L, Borri C. Frequency- and time-domain methods for the numerical modeling of full bridge aeroelasticity. Comput Struct 2007;85(11–14):675–87.
[47] Acikgoz N, Bottasso CL. A unified approach to the deformation of simplicial and non-simplicial meshes in two and three dimensions with guaranteed validity. Comput Struct 2007;85(11–14): 944–54.
[48] de Boer A, van der Schoot MS, Bijl H. Mesh deformation based on radial basis function interpolation. Comput Struct 2007;85(11–14): 784–95.
[49] Boffi D, Gastaldi L, Heltai L. On the CFL condition for the finite element immersed boundary method. Comput Struct 2007;85(11–14): 775–83.
[50] van Loon R, Anderson PD, van de Vosse FN, Sherwin SJ. Comparison of various fluid–structure interaction methods for deformable bodies. Comput Struct 2007;85(11–14):833–43.
[51] Bathe KJ. ADINA system. Encyclopedia Math 1997;11:33–5. see also www.adina.com.
[52] Zhang H, Zhang XL, Ji SH, Guo YH, Ledezma G, Elabbasi N, et al. Recent development of fluid–structure interaction capabilities in the ADINA system. Comput Struct 2003;81(8–11):1071–85.
[53] Bathe KJ. Finite element procedures. Prentice Hall; 1996.
[54] Chapelle D, Bathe KJ. The finite element analysis of shells – fundamentals. Springer; 2003.
[55] Bathe KJ, Zhang H. A flow-condition-based interpolation finite element procedure for incompressible fluid flows. Comput Struct 2002;80:1267–77.
[56] Kohno H, Bathe KJ. Insight into the flow-condition-based interpolation finite element approach: solution of steady-state advection–diffusion problems. Int J Numer Methods Eng 2005;63:197–217.
[57] Kohno H, Bathe KJ. A flow-condition-based interpolation finite element procedure for triangular grids. Int J Numer Methods Fluids 2005;49:849–75.
[58] Kohno H, Bathe KJ. A nine-node quadrilateral FCBI element for incompressible fluid flows. Commun Numer Methods Eng 2006;22: 917–31.
[59] Bathe KJ. Conserving energy and momentum in nonlinear dynamics: a simple implicit time integration scheme. Comput Struct 2007; 85(7–8):437–45.
[60] Patankar SV. Numerical heat transfer and fluid flow. Washington, DC: Hemisphere; 1980.
[61] Brezzi F, Bathe KJ. A discourse on the stability conditions for mixed finite element formulations. Comput Methods Appl Mech Eng 1990;82:27–57.
[62] Brezzi F, Fortin M. Mixed and hybrid finite element methods. Springer; 1991.
[63] Chapelle D, Bathe KJ. The inf–sup test. Comput Struct 1993;47(4/5): 537–45.
[64] Bathe KJ. The inf–sup condition and its evaluation for mixed finite element methods. Comput Struct 2001;79:243–52. p. 971.
[65] Hübner B, Walhorn E, Dinkler D. A monolithic approach to fluid–structure interaction using space-time finite elements. Comput Methods Appl Mech Eng 2004;193:2087–104.
[66] Sussman T, Bathe KJ. A finite element formulation for nonlinear incompressible elastic and inelastic analysis. Comput Struct 1987;26: 357–409.
[67] Grätsch T, Bathe KJ. Goal-oriented error estimation in the analysis of fluid flows with structural interactions. Comput Methods Appl Mech Eng 2006;195:5673–84.